J. Fluid Mech. (1986), *vol.* 171, *pp.* 121–144
Printed in Great Britain

Thin-flame theory for the combustion of a moving liquid drop: effects due to variable density

By GEORGE GOGOS,
University of Pennsylvania, Philadelphia, PA 19104, USA

S. S. SADHAL,
University of Southern California, Los Angeles, CA 90089-1453, USA

P. S. AYYASWAMY AND T. SUNDARARAJAN
Department of Mechanical Engineering and Applied Mechanics,
School of Engineering and Applied Science,
University of Pennsylvania, Philadelphia, PA 19104, USA

(Received 11 December 1984 and in revised form 14 March 1986)

The combustion of a moving liquid fuel drop has been investigated. The drop experiences a strong evaporation-induced radial velocity while undergoing slow translation. In view of the high evaporation velocity, the flow field is not in the Stokes regime. The combustion process is modelled by an indefinitely fast chemical reaction rate.

While the flow and the transport in the continuous phase and the drop internal circulation are treated as quasisteady, the drop heat-up is regarded as a transient process. The transport equations of the continuous phase require analysis by a singular perturbation technique. The transient heat-up of the drop interior is solved by a series-truncation numerical method. The solution for the total problem is obtained by coupling the results for the continuous and dispersed phases.

The enhancement in the mass burning rate and the deformation of the flame shape due to drop translation have been predicted. The initial temperature of the drop and the subsequent heating influence the temporal variations of the flamefront standoff ratio and the flame distance. The friction drag, the pressure drag and the drag due to interfacial momentum flux are individually predicted, and the total drag behaviour is discussed. The circulation inside the drop decreases with evaporation rate. A sufficiently large non-uniform evaporation velocity causes the circulation to reverse.

1. Introduction

The study of drop combustion is an important step in understanding, designing and evaluating the performance of combustion systems. Here we investigate the hydrodynamics and heat/mass transfer associated with the burning of a fuel drop that is translating in an oxidant environment. The effect of translation is brought into focus through its introduction as a perturbation to an otherwise stationary burning drop. The convective flow is such that an envelope diffusion flame is established.

There are many excellent and authoritative reviews on the subject of drop combustion (Williams 1973; Faeth 1977; Law 1982; Buckmaster & Ludford 1982; Sirignano 1983; Williams 1985). Of particular relevance to this study is the

theoretical work of Fendell, Sprankle & Dodson (1966), who considered drop combustion in the presence of a forced flow field that was entirely in the Stokes regime. However, in view of the large magnitude of the radial velocity (induced by evaporation) that usually accompanies drop burning (Law 1982), this restriction may not be met.

In the present study the effects of large radial velocity on a moving burning drop are examined by retaining both the viscous and the inertial terms in the governing equations. The effects of initial heat-up of the drop on combustion quantities of interest such as flamefront standoff ratio, flame distance and interfacial heat transport have been investigated. We approximate the continuous phase as quasi-steady while the dispersed phase is unsteady. The quasisteady nature of the continuous phase admits an asymptotic approach. The corresponding energy and species equations in Shvab–Zeldovich variables are solved through a singular perturbation matched-asymptotic technique. The transient heat-up of the drop interior is solved by a series-truncation method and is carefully matched at the interface with the continuous-phase solutions.

In §2 the density is evaluated at a suitable reference level of temperature. Later this assumption is relaxed and the effects of variable density on the mass burning rate and the drag the drop experiences are investigated.

2. Thin-flame theory: constant density

2.1. *Theoretical formulation*

Consider a single-component fuel drop of initial radius R_0 translating at an initial velocity $U_{\infty,0}$, with a fully developed internal motion, in an infinite expanse of oxidant. The drop is initially cold at a temperature T_0. The ambient temperature T_∞ and the oxidant mass fraction $(Y_0)_\infty$ are prescribed. The convective flow is slow, so that an envelope flame is established. An indefinitely fast chemical reaction rate is assumed for the combustion process. The burning zone may then be modelled as a mathematical interface where the reactants meet in stoichiometric proportion (figure 1).

The gas-phase processes and the drop internal motion will be assumed to be quasi-steady. However, the liquid heating will be treated as transient (Sundararajan & Ayyaswamy 1984). The drop shape is considered to be spherical throughout this combustion study. This is because the Weber number and the Eötvös number are very small. For analytical convenience, the density is considered fixed and is evaluated at a reference temperature. A single effective binary diffusion coefficient D_g is used for all pairs of species (Knuth 1959). Further simplification in the analysis results if the Shvab–Zeldovich formulation is employed, which requires that the Lewis number be unity. Natural convection and second-order diffusion effects are considered negligible.

With these approximations, we write the governing equations as follows.

For the gaseous phase

$$\nabla \cdot \boldsymbol{u} = 0, \tag{1a}$$

$$\boldsymbol{u} \cdot \nabla \boldsymbol{u} + \frac{1}{\rho_g} \nabla p = \nu_g \nabla^2 \boldsymbol{u}, \tag{1b}$$

$$\boldsymbol{u} \cdot \nabla T - D_g \nabla^2 T = \frac{\Delta H_c}{\rho_g c_{pg}} \omega, \tag{1c}$$

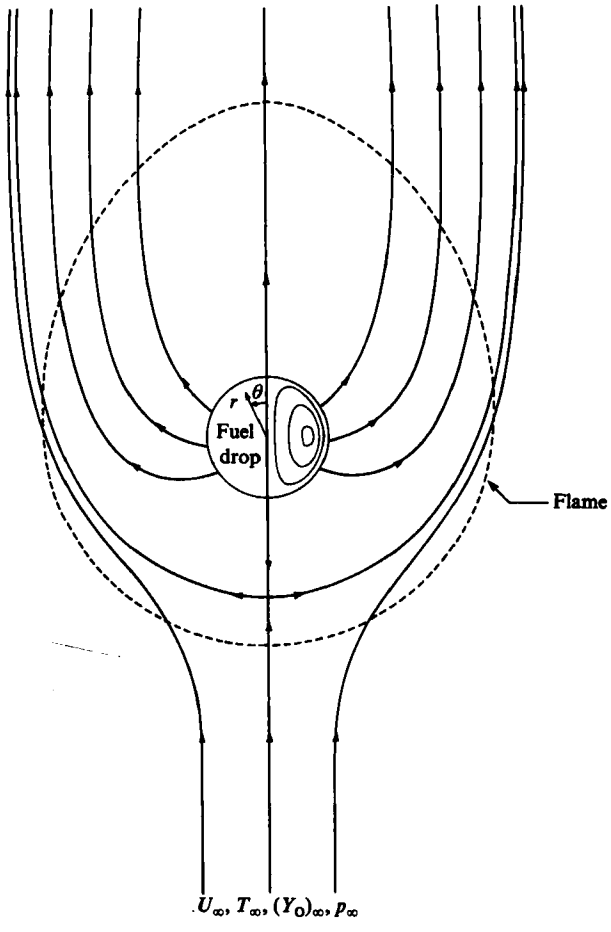

FIGURE 1. Geometry and coordinate system.

$$\boldsymbol{u}\cdot\nabla Y_{\mathrm{O}} - D_{\mathrm{g}}\nabla^2 Y_{\mathrm{O}} = -\frac{W_{\mathrm{O}}\nu_{\mathrm{O}}\omega}{\rho_{\mathrm{g}}}, \tag{1d}$$

$$\boldsymbol{u}\cdot\nabla Y_{\mathrm{F}} - D_{\mathrm{g}}\nabla^2 Y_{\mathrm{F}} = -\frac{W_{\mathrm{F}}\nu_{\mathrm{F}}\omega}{\rho_{\mathrm{g}}}, \tag{1e}$$

where ω is the reaction rate for the process

$$\nu_{\mathrm{O}}\,\mathrm{O} + \nu_{\mathrm{F}}\,\mathrm{F} \rightarrow \sum_{i=1}^{N} \nu_{\mathrm{P}_i}\,\mathrm{P}_i.$$

In the above, $\boldsymbol{u}$ is the velocity, T is the temperature, Y_{O} and Y_{F} are the mass fractions of oxidant and fuel, p is the pressure, ν_{O}, ν_{F} and ν_{P_i} are the stoichiometric coefficients of oxidant, fuel and the ith product, ΔH_{c} is the specific heat released through combustion,

$$\Delta H_{\mathrm{c}} = W_{\mathrm{O}}\nu_{\mathrm{O}}h_{\mathrm{O}} + W_{\mathrm{F}}\nu_{\mathrm{F}}h_F - \sum_{i=1}^{N-2} W_{\mathrm{P}_i}\nu_{\mathrm{P}_i}h_{\mathrm{P}_i}$$

$h_{\rm O}$, $h_{\rm F}$ and $h_{{\rm P}_i}$ are the specific heats of formation of oxidant, fuel and the *ith* product. $W_{\rm O}$, $W_{\rm F}$ and $W_{{\rm P}_i}$ are the molecular weights of oxidant, fuel and products, and $\rho_{\rm g}$, c_{pg} and $\nu_{\rm g}$ are the density, specific heat and kinematic viscosity of the mixture.

The liquid-phase equations (subscript ℓ denotes liquid side) are the same as in Chung, Ayyaswamy & Sadhal (1984, hereafter referred to as I).

We now put the governing equations in dimensionless form. The velocity and pressure for both phases are perturbed and made dimensionless as in Sadhal & Ayyaswamy (1983). The other dimensionless or stoichiometrically adjusted variables are defined as follows:

$$T^* = \frac{TW_{\rm F}c_{pg}}{\Delta H_{\rm c}}, \quad Y_{\rm O}^* = \frac{W_{\rm F}}{\nu_{\rm O}W_{\rm O}}Y_{\rm O}, \quad Y_{\rm F}^* = \frac{Y_{\rm F}}{\nu_{\rm F}}, \quad r^* = \frac{r}{R},$$

$$T_\ell^* = \frac{T_\ell W_{\rm F}c_{pg}}{\Delta H_{\rm c}}, \quad {\rm d}t^* = \frac{\alpha_\ell\,{\rm d}t}{R^2}, \quad \boldsymbol{\nabla}^* = R\boldsymbol{\nabla},$$

where α_ℓ is the liquid-phase thermal diffusivity and R is the instantaneous radius of the drop. Omitting asterisks, the quasisteady gas-phase equations in Shvab–Zeldovich form are

$$\boldsymbol{\nabla}\cdot\boldsymbol{u}' = 0, \tag{2a}$$

$$A_{00}(\boldsymbol{u}'\cdot\boldsymbol{\nabla}\boldsymbol{u}_0+\boldsymbol{u}_0\cdot\boldsymbol{\nabla}\boldsymbol{u}')+\epsilon(\boldsymbol{u}'\cdot\boldsymbol{\nabla}\boldsymbol{u}')+\boldsymbol{\nabla}p' = \boldsymbol{\nabla}^2\boldsymbol{u}', \tag{2b}$$

$$Sc\,(A_{00}\boldsymbol{u}_0+\epsilon\boldsymbol{u}')\cdot\boldsymbol{\nabla}(T+Y_{\rm O})-\boldsymbol{\nabla}^2(T+Y_{\rm O}) = 0, \tag{2c}$$

$$Sc\,(A_{00}\boldsymbol{u}_0+\epsilon\boldsymbol{u}')\cdot\boldsymbol{\nabla}(Y_{\rm F}-Y_{\rm O})-\boldsymbol{\nabla}^2(Y_{\rm F}-Y_{\rm O}) = 0, \tag{2d}$$

where $Sc = \nu_{\rm g}/D_{\rm g}$ is the Schmidt number and $\epsilon = U_\infty R/\nu_{\rm g}$ and $A_{00} = A_0R/\nu_{\rm g}$ are the instantaneous 'translational' and 'evaporation' Reynolds numbers respectively. A_0 denotes the radial velocity at the drop surface in the absence of translation and U_∞ is the instantaneous velocity of drop translation. $A_{00}\boldsymbol{u}_0$ is the purely radial flow field and $\epsilon\boldsymbol{u}'$ represents the change in the flow field due to drop translation. In this paper we investigate situations for which $\epsilon \ll 1$. However, A_{00} could be $O(1)$. In view of this, the complete flow field is not in the Stokes flow regime. The governing equations for the liquid side are as in I.

The initial and boundary conditions in dimensionless form are as follows.

Initial condition

$$T_\ell = T_0 \quad \text{at } t = 0; \tag{3}$$

Far-field conditions ($r\to\infty$)

$$Y_0 \to (Y_0)_\infty, \tag{4a}$$

$$T \to T_\infty, \tag{4b}$$

$$u_r \to \epsilon\cos\theta, \quad u_\theta \to -\epsilon\sin\theta; \tag{4c}$$

Interface conditions (the subscript s indicates interface):

(i) continuity of tangential velocity

$$\phi_\nu\boldsymbol{u}\cdot\tilde{\boldsymbol{e}}_\theta = \boldsymbol{u}_\ell\cdot\tilde{\boldsymbol{e}}_\theta, \tag{5a}$$

(ii) continuity of shear stress

$$\phi_\nu\phi_\mu\left\{r\frac{\partial}{\partial r}\left(\frac{u_\theta}{r}\right)+\frac{1}{r}\frac{\partial u_r}{\partial\theta}\right\} = r\frac{\partial}{\partial r}\left(\frac{u_{\ell\theta}}{r}\right)+\frac{1}{r}\frac{\partial u_{\ell r}}{\partial\theta}. \tag{5b}$$

(iii) temperature continuity

$$T = T_\ell \tag{5c}$$

(iv) interfacial heat balance

$$\phi_k\left[-\frac{Sc}{Ja}u_r+\frac{\partial T}{\partial r}\right]=\frac{\partial T_\ell}{\partial r}, \tag{5d}$$

(v) impermeability condition

$$\frac{\partial Y_{\mathrm{F}}}{\partial r}=-Sc\,(\alpha_{\mathrm{F}}-Y_{\mathrm{F}})\,u_r, \tag{5e}$$

(vi) Clausius–Clapeyron equation

$$Y_{\mathrm{F,\,s}}=\frac{\alpha_{\mathrm{F}}\exp\left[\chi\left(\frac{1}{T_{\mathrm{b}}}-\frac{1}{T_{\mathrm{s}}}\right)\right]}{r_{\mathrm{w}}-(r_{\mathrm{w}}-1)\exp\left[\chi\left(\frac{1}{T_{\mathrm{b}}}-\frac{1}{T_{\mathrm{s}}}\right)\right]}. \tag{5f}$$

The condition of axisymmetry is applied for all solution variables on the axis of the drop. For $\theta = 0$ and π

$$\begin{aligned} u_\theta &= \frac{\partial u_r}{\partial\theta}=\frac{\partial p}{\partial\theta}=\frac{\partial T}{\partial\theta}=\frac{\partial Y_{\mathrm{F}}}{\partial\theta}=\frac{\partial Y_{\mathrm{O}}}{\partial\theta}=u_{\ell\theta}\\ &=\frac{\partial u_{\ell r}}{\partial\theta}=\frac{\partial p_\ell}{\partial\theta}=\frac{\partial T_\ell}{\partial\theta}=0. \end{aligned} \tag{5g}$$

In the above

$$\phi_k=\frac{k_{\mathrm{g}}}{k_\ell},\quad \phi_\mu=\frac{\mu_{\mathrm{g}}}{\mu_\ell},\quad \phi_\nu=\frac{\nu_{\mathrm{g}}}{\nu_\ell},\quad Ja=\frac{\Delta H_{\mathrm{c}}}{W_{\mathrm{F}}L},$$

$$\alpha_{\mathrm{F}}=\frac{1}{\nu_{\mathrm{F}}},\quad \chi=\frac{L}{R^0}\frac{W_{\mathrm{F}}c_{pg}}{\Delta H_{\mathrm{c}}},\quad r_{\mathrm{w}}=\frac{W_{\mathrm{NF}}}{W_{\mathrm{F}}},$$

L is the latent heat of evaporation, T_{b} is the boiling temperature of the fuel corresponding to the prevailing pressure p, k is the thermal conductivity, μ is the viscosity, R^0 is the universal gas constant and W_{NF} is the average molecular weight of the non-fuel species.

According to the Burke–Schumann model,

$$Y_{\mathrm{F}}=0\quad\left(\frac{R_{\mathrm{f}}}{R}\leqslant r<\infty\right), \tag{6a}$$

$$Y_{\mathrm{O}}=0\quad\left(1\leqslant r\leqslant\frac{R_{\mathrm{f}}}{R}\right), \tag{6b}$$

where R_{f} is the flame position, which is to be determined by applying (6*a*, *b*) to the solution of (2*c*, *d*).

2.2. *Gas-phase energy and species equations*

In a different context, the solutions for the flow field for order ϵ have been given by Sadhal & Ayyaswamy (1983). We use those solutions and proceed to solve the energy and species equations. For convenience, we define

$$g=\frac{T-T_\infty+Y_{\mathrm{O}}-(Y_{\mathrm{O}})_\infty}{T_0-T_\infty-(Y_{\mathrm{O}})_\infty},\quad h=Y_{\mathrm{F}}-Y_{\mathrm{O}}+(Y_{\mathrm{O}})_\infty,\quad g_\ell=\frac{T_\ell-T_\infty-(Y_{\mathrm{O}})_\infty}{T_0-T_\infty-(Y_{\mathrm{O}})_\infty}. \tag{7a–c}$$

In terms of these transformed variables the transport equations are

$$\frac{1}{r^2}\frac{\partial}{\partial r}\left(r^2\frac{\partial g}{\partial r}\right)+\frac{1}{r^2}\frac{\partial}{\partial \mu}\left[(1-\mu^2)\frac{\partial g}{\partial \mu}\right]=Sc\left[\left(\frac{A_{00}}{r^2}+\epsilon u_{1r}\right)\frac{\partial g}{\partial r}-\epsilon\frac{u_{1\theta}}{r}(1-\mu^2)^{\frac{1}{2}}\frac{\partial g}{\partial \mu}\right], \tag{8}$$

with a similar equation for h. The quantities u_{1r} and $u_{1\theta}$ are the flow-field solutions of order ϵ (see I) and $\mu=\cos\theta$. The boundary conditions are

$$\left.\begin{aligned} g &= g_\ell, && (9a)\\ \phi_k\left\{-\frac{Sc\,(A_{00}+\epsilon u_{1r})}{Ja\,[T_0-T_\infty-(Y_O)_\infty]}+\frac{\partial g}{\partial r}\right\} &= \frac{\partial g_\ell}{\partial r}, && (9b)\\ -Sc\,[A_{00}+\epsilon u_{1r}]\,[\alpha_F+(Y_O)_\infty-h] &= \frac{\partial h}{\partial r} && (9c)\end{aligned}\right\} \text{at} \quad r=1,$$

$$g\to 0, \quad h\to 0 \quad \text{as} \quad r\to\infty. \tag{10}$$

Axisymmetry requires that

$$\left|\frac{\partial g}{\partial \mu}\right|<\infty, \quad \left|\frac{\partial h}{\partial \mu}\right|<\infty \quad \text{on} \quad \mu=\pm 1. \tag{11}$$

The equations are expanded in terms of the small parameter ϵ, and Legendre functions of μ and are solved in a manner similar to that in I. Owing to the structural similarity between the two equations governing the functions g and h, the solution techniques for both cases are the same. Therefore only the details for the solution of g are provided. We assume general forms for the inner expansions to be

$$g(r,\mu;\epsilon)=\sum_{n=0}^{\infty} f_n(\epsilon)\,g_n(r,\mu)=\sum_{n=0}^{\infty}\sum_{m=0}^{\infty} f_n(\epsilon)\,l_{mn}(r)\,P_m(\mu). \tag{12}$$

The boundary conditions at the interface are given by (9*a–c*). However, we shall first assume arbitrary values imposed at the interface, such as

$$g(1,\mu;\epsilon)=\sum_{n=0}^{\infty}\sum_{m=0}^{\infty} f_n(\epsilon)\,g_{smn}\,P_m(\mu). \tag{13}$$

In the above, $P_m(\mu)$ is the Legendre polynomial of order m. Next, we introduce $\delta=r\epsilon$ as a strained radial coordinate for the outer region and consider outer expansions of the form

$$G(\delta,\mu,\epsilon)=\sum_{n=0}^{\infty} F_n(\epsilon)\,G_n(\delta,\mu). \tag{14}$$

The complete zeroth-order solutions are

$$g_0(r,\mu)=g_{s00}\,\frac{e^{-\tilde{A}_{00}/r}-1}{e^{-\tilde{A}_{00}}-1}, \tag{15}$$

$$G_0(\delta,\mu)=-\frac{g_{s00}\,\tilde{A}_{00}\,e^{-\frac{1}{2}Sc\,\delta(1-\mu)}}{\delta(e^{-\tilde{A}_{00}}-1)}, \tag{16}$$

where $\tilde{A}_{00}=A_{00}Sc$. The next-order inner solution obtained from (12) is of the form

$$g_1(r,\mu)=\sum_{m=0}^{\infty} l_{m1}(r)\,P_m(\mu). \tag{17}$$

Here it is sufficient to retain only terms corresponding to $m = 0$ and $m = 1$, because the velocity field is calculated up to $m = 1$. The solutions are

$$l_{01}(r) = -\frac{\tilde{C}}{\tilde{A}_{00}^2}\left[e^{-\tilde{A}_{00}/r}\left(1+\frac{\tilde{A}_{00}}{r}\right)\right]+C_{11}\,e^{-\tilde{A}_{00}/r}+C_{12}, \tag{18}$$

$$l_{11}(r) = [C_{21}+\overline{V}(r)]\,e^{-\tilde{A}_{00}/r}(r+\tfrac{1}{2}\tilde{A}_{00})+[C_{22}+\overline{U}(r)]\,(r-\tfrac{1}{2}\tilde{A}_{00}), \tag{19}$$

where $\tilde{C}$, $\overline{V}(r)$, $\overline{U}(r)$ and the constants of integration C_{11}, C_{12}, C_{21} and C_{22} are as given in I, with g_{s00}, g_{s01} and g_{s11} replacing t_{i00}, t_{i01} and t_{i11} respectively. We may now obtain a uniformly valid expression for the function g as

$$g = g_0+\epsilon(g_1+G_0)+\frac{g_{s00}\,\tilde{A}_{00}}{e^{-\tilde{A}_{00}}-1}\left[\frac{1}{r}+\tfrac{1}{2}\epsilon\,Sc\,(\mu-1)\right]+o(\epsilon). \tag{20}$$

The solution for the coupling function h is identical with that for g, except that g_{s00}, g_{s01} and g_{s11} should be replaced by h_{s00}, h_{s01} and h_{s11} respectively.

The normal velocity at the drop surface is given by $u_r = A_{00}+\epsilon(A_{01}+\mu A_{11})$. It is related to the transformed fuel mass fraction (function h) at the drop surface through the impermeability condition (9*c*),

$$A_{00} = -\frac{1}{Sc}\ln\left[1-\frac{h_{s00}}{\alpha_F+(Y_O)_\infty}\right], \tag{21a}$$

$$A_{01} = \frac{h_{s01}}{Sc\,[\alpha_F+(Y_O)_\infty-h_{s00}]}-\tfrac{1}{2}\ln\left[1-\frac{h_{s00}}{\alpha_F+(Y_O)_\infty}\right], \tag{21b}$$

$$A_{11} = \frac{1}{(1-\frac{1}{2}\tilde{A}_{00})-e^{-\tilde{A}_{00}}(1+\frac{1}{2}\tilde{A}_{00})}\left\{\frac{\tilde{A}_{00}^3}{4}(1+\Omega)+\frac{A_{00}(1-\frac{1}{2}\tilde{A}_{00})+(e^{-\tilde{A}_{00}}-1)}{[\alpha_F+(Y_O)_\infty]\,e^{-\tilde{A}_{00}}}h_{s11}\right\}, \tag{21c}$$

where the constant Ω is given in I.

In the above equations the quantities h_{s00}, h_{s01} and h_{s11} are related to the drop surface temperature through (7*b*) and the Clasius–Clapeyron equation (5*f*). In view of (13), the fuel mass fraction and temperature at the drop surface can be expanded as

$$Y_{F,s} = -(Y_0)_\infty+h_{s00}+\epsilon(h_{s01}+\mu h_{s11}), \tag{22a}$$

$$T_s = T_{00}+\epsilon(T_{01}+\mu T_{11}). \tag{22b}$$

Substituting these expressions into (5*f*) and expanding in ϵ, we obtain

$$h_{s00} = (Y_O)_\infty+\frac{\alpha_F\exp\left[\chi\left(\frac{1}{T_b}-\frac{1}{T_{00}}\right)\right]}{r_w-(r_w-1)\exp\left[\chi\left(\frac{1}{T_b}-\frac{1}{T_{00}}\right)\right]}, \tag{23a}$$

$$h_{s01} = [h_{s00}-(Y_O)_\infty]\,\frac{T_{01}}{T_{00}^2}\chi, \tag{23b}$$

$$h_{s11} = [h_{s00}-(Y_O)_\infty]\,\frac{T_{11}}{T_{00}^2}\chi. \tag{23c}$$

The quantities T_{00}, T_{01} and T_{11} are obtained from the transient solution of the drop interior. The quasisteady flow and transport solutions may then be obtained for any time. The solution procedure for the transport inside the drop is described in §2.3.

2.3. *Transient heat-up of the drop interior*

We adopt the semianalytical method of series truncation for the transient solution of the liquid phase. The details are described in I, with g_ℓ and g replacing T_ℓ and T. The solution provides an updated temperature profile for both the drop surface and its interior. With this new drop-surface-temperature solution, the continuous-phase calculation for the new time-step may be effected.

2.4. *Physical quantities*

In this subsection, equations are presented for obtaining the stream function, the drag experienced by the drop, the mass burning rate, the interfacial heat transport and the velocity of the drop moving in gravitational field. The dimensionless stream function for the continuous phase is given by

$$\frac{\partial \psi}{\partial \theta} = u_r r^2 \sin\theta, \quad \frac{\partial \psi}{\partial r} = -u_\theta r \sin\theta. \tag{24a, b}$$

Similar expressions hold for the liquid side. The drag force on the liquid drop (non-dimensionalized with the Stokes drag $6\pi\mu_g U_\infty R$) consists of contributions from the viscous stresses, the pressure field and the momentum flux at the interface. These contributions to the drag may be written as follows

viscous drag

$$F_\mu = -\frac{2}{9}\frac{[(3+2\phi_\mu)-A_{11}(1+2\phi_\mu)][(2+2A_{00}+A_{00}^2)\,\mathrm{e}^{-A_{00}}-2]}{-1+\frac{1}{6}(3+2\phi_\mu)A_{00}^2+(1+A_{00}-\frac{1}{3}\phi_\mu A_{00}^2)\,\mathrm{e}^{-A_{00}}}; \tag{25a}$$

pressure drag

$$F_p = \frac{2}{9}\left\{A_{00}A_{11}+\frac{[(3+2\phi_\mu)-A_{11}(1+2\phi_\mu)][(2+A_{00})\,\mathrm{e}^{-A_{00}}+A_{00}-2]}{-1+\frac{1}{6}(3+2\phi_\mu)A_{00}^2+(1+A_{00}-\frac{1}{3}\phi_\mu A_{00}^2)\,\mathrm{e}^{-A_{00}}}\right\}; \tag{25b}$$

drag due to the momentum flux at the interface

$$F_m = \frac{2}{9}\left\{-A_{00}(3+A_{11})+\frac{[3+2\phi_\mu-A_{11}(1+2\phi_\mu)][(A_{00}+A_{00}^2)\,\mathrm{e}^{-A_{00}}-A_{00}+\frac{1}{2}A_{00}^3]}{-1+\frac{1}{6}(3+2\phi_\mu)A_{00}^2+(1+A_{00}-\frac{1}{3}\phi_\mu A_{00}^2)\,\mathrm{e}^{-A_{00}}}\right\}; \tag{25c}$$

total drag

$$F_T = -\frac{2}{9}\left(3A_{00}+\frac{C}{2A_{00}}\right), \tag{25d}$$

where C is defined in I.

The mass burning rate (dimensional) at the droplet surface is given by

$$\dot{m} = 2\pi R^2 \rho_g \frac{\nu_g}{R}\int_{-1}^{1} u_r(1,\mu,\epsilon)\,\mathrm{d}\mu. \tag{26}$$

Substituting the expansion for the radial velocity into (26),

$$\frac{\dot{m}}{\dot{m}_0} = 1+\epsilon\frac{A_{01}}{A_{00}}+\ldots, \quad \dot{m}_0 = 4\pi R\mu_g A_{00}. \tag{27}$$

The evaporation constant K is defined as

$$K = \frac{\mathrm{d}(D^2)}{\mathrm{d}t} = -\frac{2\dot{m}}{\pi\rho_\ell R}. \tag{28}$$

Using (27) and (28), the drop regression rate is given by

$$\frac{\mathrm{d}}{\mathrm{d}t}\left(\frac{D^2}{D_0^2}\right) = -\frac{8k_g \tilde{A}_{00}}{\rho_\ell c_{pg} D_0^2}\left[1+\frac{A_{01}}{A_{00}}\epsilon+o(\epsilon)\right]. \tag{29}$$

Here D and D_0 refer to the instantaneous and initial drop diameters.

The dimensionless heat transferred from the continuous phase to the drop is

$$q_g = -[T_0-T_\infty-(Y_O)_\infty]\frac{\tilde{A}_{00}\,\mathrm{e}^{-\tilde{A}_{00}}}{(R_0/R)}\left[\frac{g_{s00}}{\mathrm{e}^{-\tilde{A}_{00}}-1}+\epsilon\left(C_{11}-\frac{\tilde{C}}{\tilde{A}_{00}}\right)\right]. \tag{30a}$$

The heat required for fuel evaporation is

$$q_e = -\frac{Sc}{Ja}\frac{A_{00}+\epsilon A_{01}}{R_0/R}. \tag{30b}$$

Interfacial heat balance provides an equation for the heat q_ℓ transported into the liquid side:

$$q_\ell = q_g - q_e. \tag{30c}$$

The above heat-transfer quantities have been non-dimensionalized with $4\pi R_0 k_g \Delta H_c / W_F c_{pg}$. Balancing the forces acting on the drop (weight, drag, buoyancy and inertia), an equation for the velocity of the moving drop is obtained. In dimensionless form,

$$\frac{\mathrm{d}U_\infty}{\mathrm{d}t}-\phi_\mu Pr_\ell\left[3A_{00}+\frac{C}{2A_{00}}\right]U_\infty = \frac{g Pr_\ell R_0}{\nu_g^2}R^2(\phi_\nu-\phi_\mu), \tag{31}$$

where U_∞ has been made dimensionless with ν_g/R_0. Pr_ℓ is the liquid-phase Prandtl number and g here is the acceleration due to gravity.

3. Thin-flame theory: variable density

3.1. *Theoretical formulation*

The fixed-density assumption in §2 is a restrictive one, since temperature variations induce changes in the density of the same order of magnitude. Indeed, such an assumption has often been made in order to study the thermodiffusive properties of flames. However, if the interaction of the hydrodynamic field and the associated heat- and mass-transfer problem is of primary interest, a fixed-density model is insufficient. In this section we investigate the effects of variable density on the mass burning rate, the circulation inside the drop and on the drag that a moving isothermal burning drop experiences. The method of approach is the same as before. Since the effect of a translational motion has been introduced in our study as a perturbation to an otherwise stationary burning droplet, the scheme used in §2 could be applied to a variable-density flow field as well because the underlying radial flow field (the leading term in the expansion) is known for a variable density. However, the results of Sadhal & Ayyaswamy (1983) for the velocity field are not applicable to the variable-density problem.

We non-dimensionalize the density $\bar{\rho}_g(r,\mu)$ with ρ_g as defined in §2. The overbar indicates that the density is the considered variable. The Shvab–Zeldovich variable g is defined as before, but T_0 is replaced by T_{00}. The pressure is perturbed similarly,

$$p-p_\infty = p_0+p', \quad p_\ell-p_\infty = p_{\ell 0}+p'_\ell,$$

and scaled as follows:

$$p^* = \frac{(p-p_\infty)R^2}{\mu_g \nu_g}, \quad p_\ell^* = \frac{(p_\ell - p_\infty)R^2}{\mu_\ell \nu_\ell}.$$

All other quantities are non-dimensionalized as in §2. The product of the density and the mass diffusivity has been taken as constant ($\bar{\rho}_g \bar{D}_g = \bar{\rho}_{g,\infty} \bar{D}_{g,\infty}$). The combustion approximation is adopted, i.e. the pressure is constant everywhere except in the momentum equation (Buckmaster & Ludford 1982). The governing dimensionless equations under these circumstances become as follows.

For the gaseous phase

$$\nabla \cdot [\bar{\rho}_g \boldsymbol{u}] = 0, \tag{32a}$$

$$\bar{\rho}_g \boldsymbol{u} \cdot \nabla \boldsymbol{u} = -\nabla p + \nabla^2 \boldsymbol{u} + \tfrac{1}{3}\nabla(\nabla \cdot \boldsymbol{u}), \tag{32b}$$

$$\tilde{S}c \bar{\rho}_g \boldsymbol{u} \cdot \nabla g - \nabla^2 g = 0, \tag{32c}$$

$$\tilde{S}c \bar{\rho}_g \boldsymbol{u} \cdot \nabla h - \nabla^2 h = 0, \tag{32d}$$

$$\bar{\rho}_{g,\infty} T_\infty = \bar{\rho}_g T, \tag{32e}$$

where

$$\tilde{S}c = \frac{1}{\bar{\rho}_{g,\infty}} \frac{\nu_g}{\bar{D}_{g,\infty}}.$$

The Mach number

$$M = \left\{ \gamma \frac{(U_\infty^2/p_\infty)}{\bar{\rho}_{g,\infty}} \frac{(T_\infty/\Delta H_c)}{W_F c_{pg}} \right\}^{\frac{1}{2}}$$

(in dimensional quantities) is very small; here $\gamma = c_{pg}/c_{vg}$ the ratio of specific heats.

For the liquid phase the same equations governing the flow apply. However, some boundary conditions are modified owing to the variable density. These are as follows:

heat-flux continuity

$$\frac{\tilde{S}c}{Ja[T_{00} - T_\infty - (Y_0)_\infty]} \bar{\rho}_g(1,\mu) u_r(1,\mu) = \frac{\partial g(1,\mu)}{\partial r}; \tag{33a}$$

impermeability condition

$$\frac{\partial h(1,\mu)}{\partial r} = -\tilde{S}c \bar{\rho}_g(1,\mu) u_r(1,\mu) [\alpha_F + (Y_O)_\infty - h(1,\mu)]; \tag{33b}$$

inner expansions

$$\boldsymbol{u}(r,\mu;\epsilon) = \hat{\boldsymbol{e}}_r \{A_{00} u_0(r) + \epsilon[u_{01}(r) + \mu u_{11}(r)]\} + \hat{\boldsymbol{e}}_\theta \epsilon u_{\theta 1}(r)(1-\mu^2)^{\frac{1}{2}} + \ldots, \tag{34a}$$

$$p(r,\mu;\epsilon) = A_{00} p_0 + \epsilon[p_{01}(r) + \mu p_{11}(r)] + \ldots, \tag{34b}$$

$$\bar{\rho}_g(r,\mu;\epsilon) = \rho_0(r) + \epsilon[\rho_{01}(r) + \mu \rho_{11}(r)] + \ldots, \tag{34c}$$

$$g(r,\mu;\epsilon) = g_0(r) + \epsilon[g_{01}(r) + \mu g_{11}(r)] + \ldots, \tag{34d}$$

$$h(r,\mu;\epsilon) = h_0(r) + \epsilon[h_{01}(r) + \mu h_{11}(r)] + \ldots, \tag{34e}$$

$$T(r,\mu;\epsilon) = T_0(r) + \epsilon[T_{r01}(r) + \mu T_{r11}(r) + \ldots; \tag{34f}$$

outer expansions

$$\boldsymbol{u}(\delta,\mu;\epsilon) = \epsilon\hat{\boldsymbol{\imath}}+\epsilon^2\boldsymbol{U}(\delta,\mu)+\ldots, \tag{35a}$$

$$p(\delta,\mu;\epsilon) = \epsilon^3 P(\delta,\mu)+\ldots, \tag{35b}$$

$$\bar{\rho}_{\mathrm{g}}(\delta,\mu;\epsilon) = \bar{\rho}_{\mathrm{g},\infty}+\epsilon\bar{R}(\delta,\mu)\ldots, \tag{35c}$$

$$g(\delta,\mu;\epsilon) = \epsilon G(\delta,\mu)+\ldots, \tag{35d}$$

$$h(\delta,\mu;\epsilon) = \epsilon H(\delta,\mu)+\ldots, \tag{35e}$$

$$T(\delta,\mu;\epsilon) = T_\infty+\epsilon\bar{T}(\delta,\mu)+\ldots, \tag{35f}$$

Substitution of the inner expansions (34*a–e*) into the governing equations (32*a–e*) leads to the sphericosymmetric problem and two boundary-value problems of order ϵ. The zeroth-order problem is solved analytically. The radially symmetric terms of order ϵ lead to a linear two-point boundary-value problem. It is solved analytically through matching with the outer solution, and an expression for the mass burning rate is provided. The second problem is a two-point linear boundary-value problem which describes deviation from radial symmetry due to the presence of forced convection. The solution is obtained numerically and provides the modification to Stokes drag due to mass transfer. The analytical zeroth-order solution is used to facilitate computations. The boundary conditions as $r\to\infty$ are provided from the outer-problem solution, which is obtained analytically. The governing equations for the leading-order outer problem are obtained by substituting (35*a–e*) into (32*a–e*).

3.2. *Lowest-order inner and outer solutions*

The zeroth-order sphericosymmetric problem is governed by the following set of equations:

$$\frac{\mathrm{d}}{\mathrm{d}r}(r^2\rho_0 u_0) = 0, \tag{36a}$$

$$A_{00}\rho_0 u_0\frac{\mathrm{d}u_0}{\mathrm{d}r} = -\frac{\mathrm{d}p_0}{\mathrm{d}r}+\frac{4}{3}\left(\frac{\mathrm{d}^2u_0}{\mathrm{d}r^2}+\frac{2}{r}\frac{\mathrm{d}u_0}{\mathrm{d}r}-\frac{2u_0}{r^2}\right), \tag{36b}$$

$$\tilde{A}'_{00}\rho_0 u_0\frac{\mathrm{d}g_0}{\mathrm{d}r}-\frac{1}{r^2}\frac{\mathrm{d}}{\mathrm{d}r}\left(r^2\frac{\mathrm{d}g_0}{\mathrm{d}r}\right) = 0, \tag{36c}$$

with a similar equation for h_0.

$$\rho_0 T_0 = \bar{\rho}_{\mathrm{g},\infty}T_\infty, \tag{36d}$$

subject to the following conditions at $r = 1$: impermeability gives:

$$\frac{\mathrm{d}h_0(1)}{\mathrm{d}r} = -\tilde{A}'_{00}\rho_0(1)\,[\alpha_{\mathrm{F}}+(Y_{\mathrm{O}})_\infty-h_{\mathrm{s00}}], \tag{37a}$$

heat-flux continuity gives

$$\frac{\tilde{A}'_{00}}{g_{\mathrm{D}}Ja}\rho_0(1) = \frac{\mathrm{d}g_0(1)}{\mathrm{d}r}, \tag{37b}$$

where $g_{\mathrm{D}} = T_{00}-T_\infty-(Y_{\mathrm{O}})_\infty$ and $\tilde{A}'_{00} = A_{00}\tilde{S}c$. The Clausius–Clapeyron equation is given by (23*a*).

The governing equations for the outer leading-order problem are

$$\nabla_\delta \cdot \hat{\imath}\overline{R} + \overline{\rho}_{g,\infty} \nabla_\delta \cdot U = 0, \tag{38a}$$

$$\overline{\rho}_{g,\infty} \hat{\imath} \cdot \nabla_\delta U = -\nabla_\delta P + \tfrac{4}{3}\nabla_\delta(\nabla_\delta \cdot U) - \nabla_\delta \times (\nabla_\delta \times U), \tag{38b}$$

$$\tilde{S}c\,\overline{\rho}_{g,\infty} \hat{\imath} \cdot \nabla_\delta G - \nabla_\delta^2 G = 0, \tag{38c}$$

$$\tilde{S}c\,\overline{\rho}_{g,\infty} \hat{\imath} \cdot \nabla_\delta H - \nabla_\delta^2 H = 0, \tag{38d}$$

$$\overline{\rho}_{g,\infty}[g_D G + H] + T_\infty \overline{R} = 0 \quad \text{(state)}. \tag{38e}$$

As $\delta \to \infty$ all dependent variables vanish. This condition together with the interface conditions (23a) and (37a, b) and the matching requirement for all variables provide the necessary relations for the solution to the inner and outer problems of leading order.

The inner lowest-order solution is presented next. From continuity,

$$r^2 \rho_0 u_0 = \rho_0(1) = M_0. \tag{39}$$

Owing to the combustion approximation, the momentum equation (36b) is decoupled from the rest of the set. It solution can provide the pressure distribution if desired. The solutions to the Shvab–Zeldovich variables g and h are obtained as in §2:

$$g_0 = g_{s00} \frac{e^{-\tilde{A}'_{00} M_0 / r} - 1}{e^{-\tilde{A}'_{00} M_0} - 1}, \tag{40}$$

with a similar expression for h_0. Heat-flux continuity leads to

$$\tilde{A}'_{00} M_0 = \ln\{1 - Ja\,[T_{00} - T_\infty - (Y_0)_\infty]\}. \tag{41}$$

From impermeability,

$$h_{s00} = [\alpha_F + (Y_O)_\infty][1 - e^{-\tilde{A}'_{00} M_0}]. \tag{42}$$

The Clausius–Clapeyron equation (23a) together with (41) and (42) are employed in an iterative procedure, which provides the drop surface quantities. The spherico-symmetric flamefront standoff ratio R_{f0}/R is obtained using (6a, b) and h_0:

$$\frac{R_{f0}}{R} = \frac{\ln\left[1 - \dfrac{h_{s00}}{\alpha_F + (Y_O)_\infty}\right]}{\ln\left[1 - \dfrac{(Y_O)_\infty}{\alpha_F + (Y_O)_\infty}\right]}. \tag{43}$$

Using (6a, b) and (7a, b), the temperature distribution is obtained as

$$T_0(r) = \begin{cases} g_D g_0(r) + T_\infty + (Y_O)_\infty & \left(1 < r < \dfrac{R_{f0}}{R}\right), \\ \\ g_D g_0(r) + h_0(r) + T_\infty & \left(\dfrac{R_{f0}}{R} < r < \infty\right). \end{cases} \tag{44}$$

The state and continuity equations provide the radial dependence of ρ_0 and u_0.

The outer solution is obtained following Fendell, Coats & Smith (1968). As $\delta \to 0$

$$g(\delta, \mu; \epsilon) \sim \frac{\pi\epsilon}{\tilde{S}c\,\bar{\rho}_{g,\infty}\,\delta}\left[1+\bar{\rho}_{g,\infty}\,\tilde{S}c\,\tfrac{1}{2}\delta(\mu-1)\right]C_0+\ldots, \tag{45a}$$

$$h(\delta, \mu; \epsilon) \sim \frac{\pi\epsilon}{\tilde{S}c\,\bar{\rho}_{g,\infty}\,\delta}\left[1+\bar{\rho}_{g,\infty}\,\tilde{S}c\,\tfrac{1}{2}\delta(\mu-1)\right]D_0+\ldots, \tag{45b}$$

$$u_r(\delta, \mu; \epsilon) \sim -\frac{\epsilon^2}{\delta^2}[K_1+B_0+\pi E_0]+\left(\epsilon-\frac{\epsilon^2\pi E_0}{\delta}\right)\mu+\ldots, \tag{45c}$$

$$u_\theta(\delta, \mu; \epsilon) \sim (1-\mu^2)\left[-\epsilon+\frac{\epsilon^2}{\delta}\left(\tfrac{1}{2}\pi E_0-K_2 K_1\right)\right]+\ldots, \tag{45d}$$

$$p(\delta, \mu; \epsilon) \sim \epsilon^2(K_3+B_0)\frac{\mu}{\delta^2}+\ldots, \tag{45e}$$

where

$$C_0 = -\frac{\tilde{A}'_{00}\,M_0\,\tilde{S}c\,\bar{\rho}_{g,\infty}}{\pi(\mathrm{e}^{-\tilde{A}'_{00}M_0}-1)}, \quad D_0 = C_0\,h_{s00},$$

$$\frac{A_{00}\,T_\infty}{T_{00}} = -(K_1+B_0+\pi E_0),$$

$$K_1 = -\frac{1}{\bar{\rho}_{g,\infty}\,T_\infty\,\tilde{S}c}\,\frac{\tilde{A}'_{00}\,M_0}{\mathrm{e}^{-\tilde{A}'_{00}M_0}-1}\,(g_D\,g_{s00}+h_{s00}),$$

$$K_2 = \tfrac{1}{2}\bar{\rho}_{g,\infty}\,\tilde{S}c,$$

$$K_3 = -\frac{K_1}{\bar{\rho}_{g,\infty}\,\tilde{S}c}\left(\frac{4}{3}-\frac{1}{\bar{\rho}_{g,\infty}\,\tilde{S}c}\right).$$

3.3. *Modification of the mass burning rate*

The dimensional mass burning rate is given by

$$\dot{m} = 2\pi R\mu_g\int_{-1}^{1}\bar{\rho}_g(1,\mu)\,u_r(1,\mu)\,\mathrm{d}\mu. \tag{46}$$

Substituting (34*a*, *c*) into (46),

$$\frac{\dot{m}}{\dot{m}_0} = 1+\epsilon\frac{\rho_0(1)\,u_{01}(1)+A_{00}\,\rho_{01}(1)}{A_{00}\,\rho_0(1)}, \tag{47}$$

where $\dot{m}_0\,(=4\pi R\mu_g\,A_{00}\,\rho_0(1))$ is the sphericosymmetric mass burning rate. The modification to the mass burning rate in the presence of forced convection depends on the radially symmetric terms u_{01} and ρ_{01}, which can be found independently of the terms associated with computation of drag. The first-order problem governing these terms is described next, and the solution is obtained through matching with the outer solution.

$$\frac{\mathrm{d}}{\mathrm{d}r}[r^2(\rho_0\,u_{01}+A_{00}\,\rho_{01}\,u_0)] = 0, \tag{48a}$$

$$A_{00}\left[\rho_0\,u_0\frac{\mathrm{d}u_{01}}{\mathrm{d}r}+(\rho_0\,u_{01}+A_{00}\,\rho_{01}\,u_0)\frac{\mathrm{d}u_0}{\mathrm{d}r}\right] = -\frac{\mathrm{d}p_{01}}{\mathrm{d}r}+\frac{4}{3}\left[\frac{\mathrm{d}^2u_{01}}{\mathrm{d}r^2}+\frac{2}{r}\frac{\mathrm{d}u_{01}}{\mathrm{d}r}-\frac{2u_{01}}{r^2}\right], \tag{48b}$$

$$\tilde{A}'_{00}\,\rho_0\,u_0\frac{\mathrm{d}g_{01}}{\mathrm{d}r}+\tilde{S}c\,(\rho_0\,u_{01}+A_{00}\,\rho_{01}\,u_0)\frac{\mathrm{d}g_0}{\mathrm{d}r}-\frac{1}{r^2}\frac{\mathrm{d}}{\mathrm{d}r}\left(r^2\frac{\mathrm{d}g_{01}}{\mathrm{d}r}\right) = 0, \tag{48c}$$

with a similar equation for h_{01},

$$\rho_{01} = -\frac{\rho_0^2 T_{r01}}{\bar{\rho}_{g,\infty} T_\infty} \quad \text{(state)}, \tag{48d}$$

subject to the following conditions at $r = 1$: heat-flux continuity gives

$$\frac{\tilde{S}c}{g_D Ja}[A_{00}\rho_{01}(1) + \rho_0(1)\, u_{01}(1)] = \frac{\mathrm{d}g_{01}(1)}{\mathrm{d}r}, \tag{49a}$$

impermeability gives

$$\frac{\mathrm{d}h_{01}(1)}{\mathrm{d}r} = \tilde{S}c\{A_{00}\rho_0(1)\, h_{s01} - [A_{00}\rho_{01}(1) + \rho_0(1)\, u_{01}(1)][\alpha_F + (Y_0)_\infty - h_{s00}]\}. \tag{49b}$$

The Clausius–Clapeyron relation is given by (23b). From matching with the outer solution (as $r \to \infty$)

$$g_{01} \to \frac{g_{s00}\tilde{A}'_{00} M_0}{\mathrm{e}^{-\tilde{A}'_{00} M_0} - 1} \tfrac{1}{2}\bar{\rho}_{g,\infty} \tilde{S}c, \tag{49c}$$

with a similar expression for h_{01}, and

$$\left.\begin{aligned} u_{01} &\to 0, \\ \rho_{01} &\to 0. \end{aligned}\right\} \text{ as } r \to \infty. \tag{49d, e}$$

Integrating the mass continuity equation gives

$$\rho_0 u_{01} + A_{00}\rho_{01} u_0 = \frac{M_{01}}{r^2}. \tag{50}$$

Then (48c) becomes

$$\frac{\mathrm{d}^2 g_{01}}{\mathrm{d}r^2} + \left(\frac{2}{r} - \frac{\tilde{A}'_{00} M_0}{r^2}\right)\frac{\mathrm{d}g_{01}}{\mathrm{d}r} = \tilde{C}' \frac{\mathrm{e}^{-\tilde{A}'_{00} M_0/r}}{r^4}, \tag{51}$$

where

$$\tilde{C}' = \frac{\tilde{S}c\, M_{01}\tilde{A}'_{00} M_0 g_{s00}}{\mathrm{e}^{-\tilde{A}'_{00} M_0} - 1}.$$

The solution to (51) is obtained through the method of variation of parameters:

$$g_{01} = -\frac{\tilde{C}'}{(\tilde{A}'_{00} M_0)^2}\mathrm{e}^{-\tilde{A}'_{00} M_0/r}\left(1 + \frac{\tilde{A}'_{00} M_0}{r}\right) + C'_{11}\mathrm{e}^{-\tilde{A}'_{00} M_0/r} + C'_{12}, \tag{52}$$

$$C'_{11} = \frac{g_{s01}}{\mathrm{e}^{-\tilde{A}'_{00} M_0} - 1} - \frac{g_{s00}\tilde{A}'_{00} M_0}{(\mathrm{e}^{-\tilde{A}'_{00} M_0} - 1)^2}\left\{\tfrac{1}{2}\bar{\rho}_{g,\infty}\tilde{S}c + \frac{\tilde{S}c\, M_{01}}{(\tilde{A}'_{00} M_0)^2}[1 - \mathrm{e}^{-\tilde{A}'_{00} M_0}(1 + \tilde{A}'_{00} M_0)]\right\}, \tag{53a}$$

$$C'_{12} = -\frac{g_{s01}}{\mathrm{e}^{-\tilde{A}'_{00} M_0} - 1} + \frac{g_{s00}\tilde{A}'_{00} M_0 \mathrm{e}^{-\tilde{A}'_{00} M_0}}{(\mathrm{e}^{-\tilde{A}'_{00} M_0} - 1)^2}\left[\tfrac{1}{2}\bar{\rho}_{g,\infty}\tilde{S}c - \frac{\tilde{S}c\, M_{01}}{\tilde{A}'_{00} M_0}\right]. \tag{53b}$$

Owing to the structural similarity, the solution to h is also given by (52) and (53a, b), with h_{s00} and h_{s01} replacing g_{s00} and g_{s01} respectively.

Using heat-flux continuity,

$$M_{01} = \tfrac{1}{2}\tilde{A}'_{00} M_0 \bar{\rho}_{g,\infty} + \frac{Ja\, T_{01}}{\tilde{S}c\,(g_D Ja - 1)}. \tag{54}$$

From impermeability and the state equation,

$$h_{s01} = -[\alpha_F + (Y_0)_\infty]\,\tilde{A}'_{00}\,M_0\,e^{-\tilde{A}'_{00}M_0}\left(\tfrac{1}{2}\rho_{g,\infty}\tilde{S}c - \frac{\tilde{S}c\,M_{01}}{\tilde{A}'_{00}\,M_0}\right). \tag{55}$$

The Clausius–Clapeyron equation (23*b*) together with (54) and (55) are employed in an iterative procedure, which provides the drop surface quantities. Combining (47), (50) and (54) gives

$$\frac{\dot{m}}{\dot{m}_0} = 1 + \epsilon\left[\tfrac{1}{2}\bar{\rho}_{g,\infty}\tilde{S}c + \frac{Ja\,T_{01}}{\tilde{A}'_{00}\,M_0(g_D\,Ja - 1)}\right]. \tag{56}$$

3.3 *Modification to Stokes drag due to mass transfer*

The dimensional drag force experienced by the drop is given by

$$\boldsymbol{F}_T = \int_S [\bar{\rho}_g\,\boldsymbol{u}\boldsymbol{u} + p\boldsymbol{I} - \boldsymbol{\sigma})]\cdot \mathrm{d}\boldsymbol{s}, \tag{57}$$

where $\boldsymbol{I}$ is the unit tensor and $\boldsymbol{\sigma}$ is the stress tensor given by

$$\boldsymbol{\sigma} = \mu_g[\nabla\boldsymbol{u} + (\nabla\boldsymbol{u})^T] - \tfrac{2}{3}\mu_g\,\boldsymbol{I}(\nabla\cdot\boldsymbol{u}). \tag{58}$$

The drag is non-dimensionalized with the Stokes drag $6\pi\mu_g\,U_\infty\,R$. Substitution of (34*a–e*) leads to the following expressions for the three contributions to the drag

viscous drag

$$F_\mu = \frac{2}{9}\left\{\frac{4}{3}\frac{\mathrm{d}u_{11}(1)}{\mathrm{d}r} + \tfrac{2}{3}[u_{11}(1) + u_{\theta 1}(1)] - 2\frac{\mathrm{d}u_{\theta 1}(1)}{\mathrm{d}r}\right\}, \tag{59}$$

pressure drag

$$F_p = -\tfrac{2}{3}p_{11}(1), \tag{60}$$

drag due to momentum flux at the interface

$$F_m = -\tfrac{2}{9}\{2A_{00}\rho_0(1)\,[u_{11}(1) - u_{\theta 1}(1)] + A_{00}^2\,\rho_{11}(1)\}. \tag{61}$$

Equations (59)–(61) indicate that the radially symmetric terms of order ϵ do not contribute to drag computations. Evaluation of the drag components necessitates solution of an eighth-order two-point boundary-layer problem obtained by substitution of (34*a–e*) into the governing equations (32*a–e*). The boundary conditions as $r \to \infty$ are derived from matching with the outer solution (45*a–e*). The boundary-value problem is given next in a form appropriate for numerical computation:

state

$$\rho_{11} = -\frac{\rho_0^2\,T_{r11}}{\bar{\rho}_{g,\infty}\,T_\infty}, \tag{62a}$$

$$\frac{\mathrm{d}u_{11}}{\mathrm{d}r} = -\left(\frac{1}{\rho_0}\frac{\mathrm{d}\rho_0}{\mathrm{d}r} + \frac{2}{r}\right)u_{11} + \frac{K_0}{r^2}\left(\frac{\mathrm{d}T_{r11}}{\mathrm{d}r} + \frac{T_{r11}}{\rho_0}\frac{\mathrm{d}\rho_0}{\mathrm{d}r}\right) - \frac{2u_{\theta 1}}{r}, \tag{62b}$$

$$\frac{\mathrm{d}^2 g_{11}}{\mathrm{d}r^2} = \left(\frac{\tilde{A}'_{00}\,M_0}{r^2} - \frac{2}{r}\right)\frac{\mathrm{d}g_{11}}{\mathrm{d}r} + \frac{2}{r^2}g_{11} - K_0\,\tilde{S}c\frac{\rho_0}{r^2}\frac{\mathrm{d}g_0}{\mathrm{d}r}T_{r11} + \tilde{S}c\,\rho_0\frac{\mathrm{d}g_0}{\mathrm{d}r}u_{11}, \tag{62c}$$

with a similar equation for h_{11},

$$\frac{\mathrm{d}^2 u_{\theta 1}}{\mathrm{d}r^2} = \left(\frac{A_{00} M_0}{r^2} - \frac{2}{r}\right)\frac{\mathrm{d}u_{\theta 1}}{\mathrm{d}r} + \frac{4}{r^2}u_{11} + \left(\frac{A_{00} M_0}{r^3} + \frac{4}{r^2}\right)u_{\theta 1} - \frac{1}{r}\frac{\mathrm{d}u_{11}}{\mathrm{d}r} + \frac{1}{r}s_{11}, \tag{62d}$$

$$\frac{\mathrm{d}s_{11}}{\mathrm{d}r} = \left(\frac{A_{00} M_0}{r^2} - \frac{4}{r}\right)\frac{\mathrm{d}u_{11}}{\mathrm{d}r} - \frac{2}{r}\frac{\mathrm{d}u_{\theta 1}}{\mathrm{d}r} - K_0 \tilde{A}'_{00}\frac{\rho_0}{r^2}\frac{\mathrm{d}u_0}{\mathrm{d}r}T_{r11} + \left(A_{00}\rho_0\frac{\mathrm{d}u_0}{\mathrm{d}r} + \frac{6}{r^2}\right)u_{11} + \frac{6}{r^2}u_{\theta 1}, \tag{62e}$$

where $$K_0 = \frac{A_{00} M_0}{\bar{\rho}_{g,\infty} T_\infty}, \quad s_{11} = -p_{11} + \frac{4}{3}\left(\frac{\mathrm{d}u_{11}}{\mathrm{d}r} - \frac{u_{11} + u_{\theta 1}}{r}\right).$$

From the thin-frame approximation (6a, b)

$$T_{r11}(r) = \begin{cases} g_{\mathrm{D}} g_{11}(r) & \left(1 < r < \dfrac{R_{\mathrm{f}}}{R}\right), \\ g_{\mathrm{D}} g_{11}(r) + h_{11}(r) & \left(\dfrac{R_{\mathrm{f}}}{R} < r < \infty\right), \end{cases}$$

subject to the following conditions at $r = 1$: heat-flux continuity gives

$$\frac{\tilde{S}c}{g_{\mathrm{D}} Ja}[A_{00}\rho_{11}(1) + \rho_0(1)\, u_{11}(1)] = \frac{\mathrm{d}g_{11}(1)}{\mathrm{d}r}, \tag{63a}$$

and impermeability gives

$$\frac{\mathrm{d}h_{11}(1)}{\mathrm{d}r} = \tilde{S}c\{A_{00}\rho_0(1)\, h_{s11} - [A_{00}\rho_{11}(1) + \rho_0(1)\, u_{11}(1)][\alpha_{\mathrm{F}} + (Y_0)_\infty - h_{s00}]\}. \tag{63b}$$

The Clausius–Clapeyron relation is given by (23c). Continuity of tangential velocity at $r = 1$ gives

$$u_{\theta 1}(1) = -\frac{\phi_\mu}{3 + \phi_\mu}\left[u_{11}(1) - \frac{\mathrm{d}u_{\theta 1}(1)}{\mathrm{d}r}\right]. \tag{63c}$$

From matching with the outer solution (as $r \to \infty$),

$$g_{11} \to -\frac{g_{s00}\tilde{A}'_{00} M_0}{\mathrm{e}^{-\tilde{A}'_{00} M_0} - 1}\tfrac{1}{2}\bar{\rho}_{\mathrm{g},\infty}\tilde{S}c, \tag{63d}$$

with a similar expression for h_{11},

$$\left.\begin{aligned} u_{11} &\to 0, \\ s_{11} &\to 0 \end{aligned}\right\} \quad \text{as } r \to \infty. \tag{63e, f}$$

4. Results and discussion

Several features of the moving-drop combustion problem have been systematically examined. These are the effects of translational velocity and a non-uniform radial velocity field, the roles played by the drop bulk temperature and the injection velocity, and the presence of liquid circulation. Mass burning rates have been predicted. The drag phenomena associated with moving burning fuel drops have been described. Flame shapes and distances have also been calculated. From a detailed transient calculation of the drop heat-up, we are able to analyse the role played by drop heating on combustion.

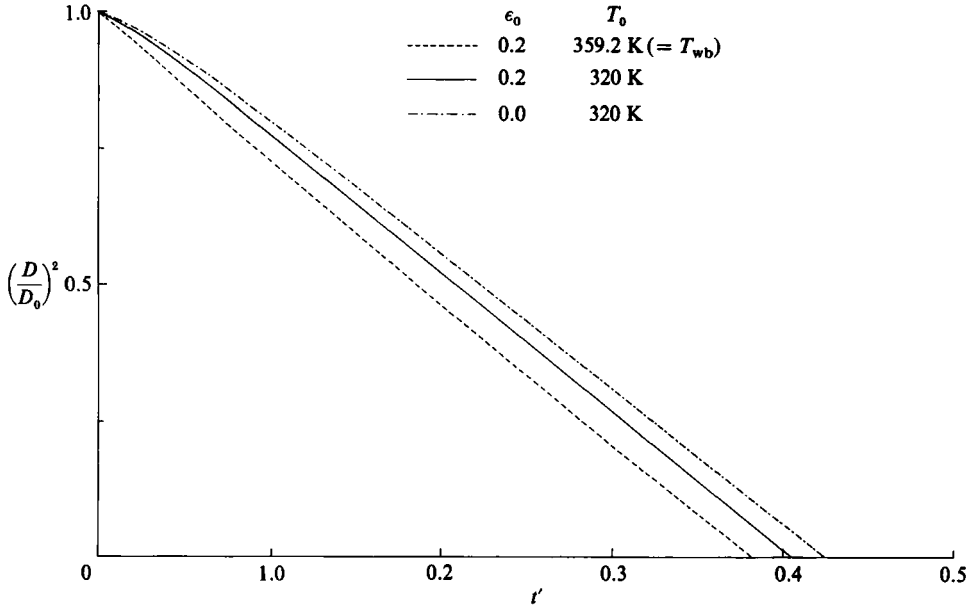

FIGURE 2. Rate of change of the square of the drop diameter with time.

We choose to present results for the combustion of an n-heptane drop burning in air. Following Law & Williams (1972), we calculate the following parameter values for this study:

$$c_{pg} = 3.64 \text{ kJ kg}^{-1} \text{ K}^{-1}, \quad \rho_g = 0.60 \text{ kg m}^{-3}, \quad \nu_g = 0.43 \times 10^{-4} \text{ m}^2 \text{ s}^{-1},$$
$$Pr = Sc = 1.0, \quad \rho_\ell = 650 \text{ kg m}^{-3}, \quad \alpha_\ell = 0.72 \times 10^{-7} \text{ m}^2 \text{ s}^{-1},$$
$$\phi_\mu = 0.1, \quad \phi_k = 0.84, \quad L = 317 \text{ kJ kg}^{-1}, \quad T_b = 371.6 \text{ K},$$
$$T_\infty = 298 \text{ K}, \quad (Y_O)_\infty = 0.23, \quad W_F = 100.2, \quad r_w = 0.3,$$
$$\nu_F = 1, \nu_0 = 11, \quad \Delta H_c = 45000 \text{ kJ kg}^{-1}.$$

The temporal variation of the square of the diameter for an n-heptane droplet is shown in figure 2 for two different drop initial temperatures T_0. For a drop initially translating with $\epsilon_0 = 0.2$ ($\epsilon_0 = U_{\infty,0} R_0/\nu_g$) and initial temperature T_0 equal to the wet-bulk temperature T_{wb} (calculated to be 359.2 K for the illustration cited), the slope of $(D/D_0)^2$ decreases continuously with t' ($= t\alpha_\ell/R_0^2$). The decrease in slope is due to the drop deceleration caused by the drag that the drop experiences. The reduction in forced convection leads to a reduced enhancement in the evaporation rate with increasing time. For $T_0 < T_{wb}$, under the same initial convective field ($\epsilon_0 = 0.2$), an initial transient drop heat-up leads to a relatively lower evaporation rate for short times ($t' < 0.1$). The droplet lifetime is prolonged as a consequence of the smaller evaporation rate for short times. The graph also shows that for the same initial temperature, the absence of translation prolongs the droplet lifetime further.

The streamlines and flame position are shown in figure 3 for two different times for an n-heptane drop with initial temperature $T_0 = 320$ K and $\epsilon_0 = 0.1$. Since the interfacial normal velocity is radially outward, streamlines emanate from the drop surface and follow the uniform stream. Near the front of the drop, the radial flow and the uniform stream oppose each other. As a result a stagnation point is formed

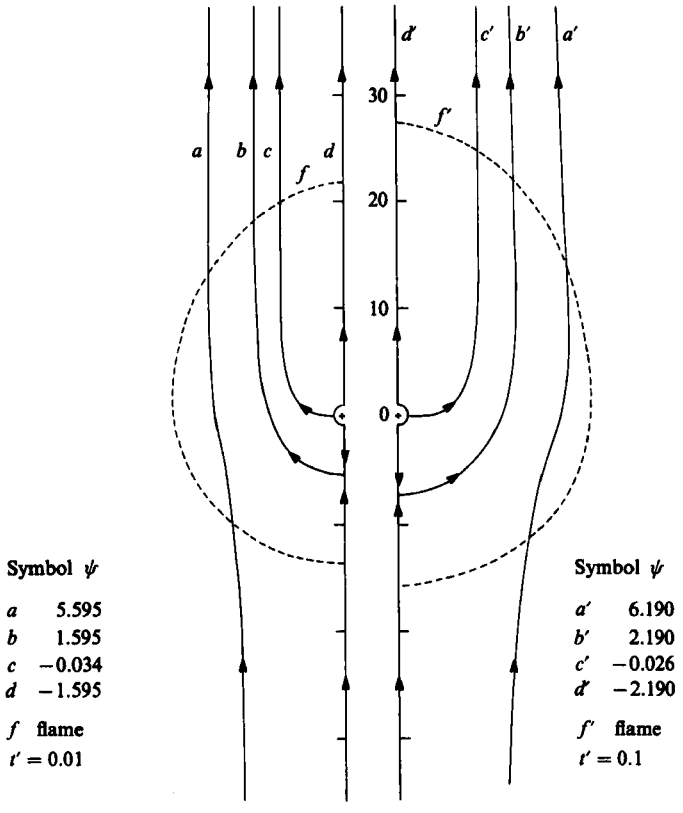

FIGURE 3. Streamlines and flame shapes at two different times.

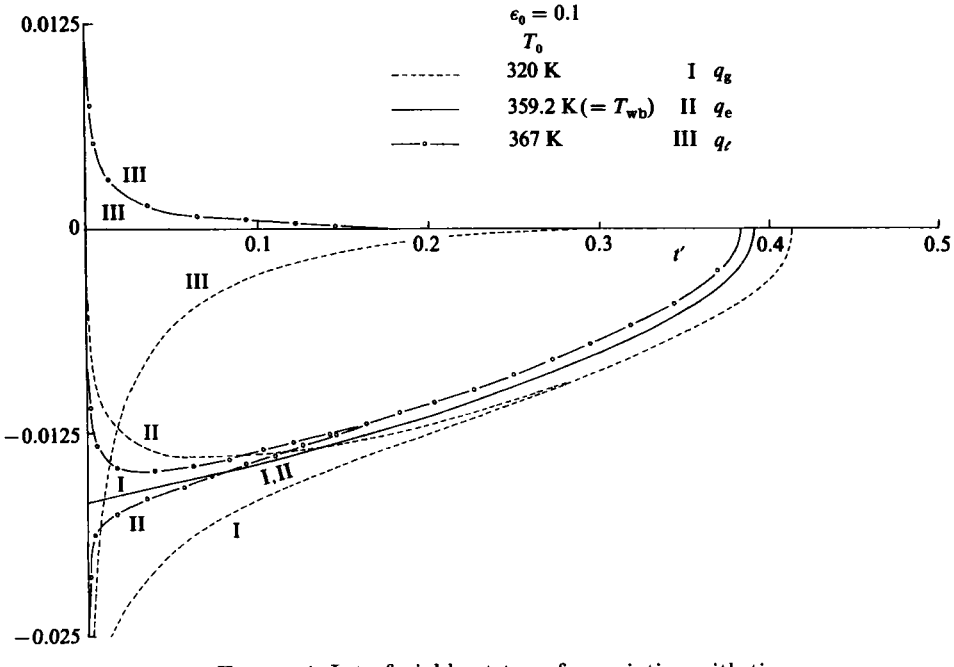

FIGURE 4. Interfacial heat-transfer variation with time.

there as shown in figure 3. For this convective situation, the stagnation point is situated between the flame and the droplet surface (Aldred, Patel & Williams 1971). For the parameters considered here, the radial field A_{00}, which is 1.492 at $t' = 0.01$, increases to 2.115 as t' becomes 0.1. This increase causes both the flame and the stagnation point to move radially outwards away from the drop. The non-sphericity in the flame shape is directly ascribable to the presence of the forced-convection field.

In figure 4 the heat transported towards the drop from the continuous phase is denoted by q_g, that required for evaporation is q_e and the heat conducted into the drop is q_ℓ. For a drop that is introduced at its wet-bulk temperature T_{wb}, heat from the continuous phase is entirely utilized for fuel evaporation. For drop initial temperatures less than the wet-bulb temperature, for some period of the drop lifetime, part of the heat input is used for fuel evaporation while the remainder is conducted to the drop interior. With increasing surface temperature T_s, while q_g decreases, q_e increases. With higher T_s, the mass fraction of the fuel at the interface is higher, leading to the increased q_e. At T_{wb}, q_g exactly balances q_e. For an initial temperature of 320 K, it is evident from the figure that for as much as a third of the drop lifetime, substantial heat from the continuous phase is being used for the drop heat-up. For drop initial temperatures higher than the wet-bulb value, the interface receives heat both from the drop interior and the continuous phase. This results in very high values for initial evaporation rates.

Figures 5(*a*, *b*) show the temporal variations of the flamefront standoff ratio R_f/R and the flame distance R_f/R_0 for different initial temperatures. The results are presented for specific angular positions ($\mu = 0, \pm 1$). In figure 5(*a*), T_0 is less than T_{wb}. Initially, there is a rapid increase in the flamefront standoff ratio. This is due to the sharp increase in the strength of the radial field (characterized predominantly by A_{00}) with higher surface temperatures. When the surface temperature attains the wet-bulb value, the radial field becomes a constant, and for $\mu = 1.0$ the ratio R_f/R almost becomes a constant. Experimental results (Law, Chung & Srinivasan 1980) on the flamefront standoff ratio show a continuously increasing trend due to fuel-vapour accumulation. The present theory does not have this feature, and therefore shows a flattening trend. For the angles $\mu = 0$ and $\mu = -1.0$ the ratio R_f/R increases continuously with time because the translational Reynolds number ϵ decreases owing to the drag and the reduction in the drop size. Towards the end of the drop lifetime, ϵ is very small, so that the flame shape is spherically symmetric. The flame distance, however, increases rapidly to a maximum value and thereafter decreases monotonically. The flame distance depends on both the radial field and the instantaneous drop radius. While the radial field causes the flame to move outwards, the drop regression leads to an inward motion. In figure 5(*b*) the drop initial temperature is higher than the wet-bulb value. Owing to the high evaporation rates during the early part of the drop lifetime, the flame is established at a distance far from the drop surface. With increasing time and for $\mu = 1.0$, as the surface temperature approaches T_{wb} the flamefront standoff ratio decreases to a constant value. Towards the end of the drop lifetime, for $\mu = 0$ and $\mu = -1.0$, a similar behaviour to that observed in figure 5(*a*) is predicted. The flame distance decreases monotonically, since both the radial field and the drop regression rate cause the flame to move inwards.

The instantaneous drag forces on a moving burning isothermal liquid drop as a function of the strength of the radial field due to evaporation are plotted in figure 6. At relatively weak radial fields the drag decreases to a minimum. With a further increase in A_{00} the drag increases. The decrease in drag is due to vorticity being convected away from the surface, and to the reduction in the pressure drop between

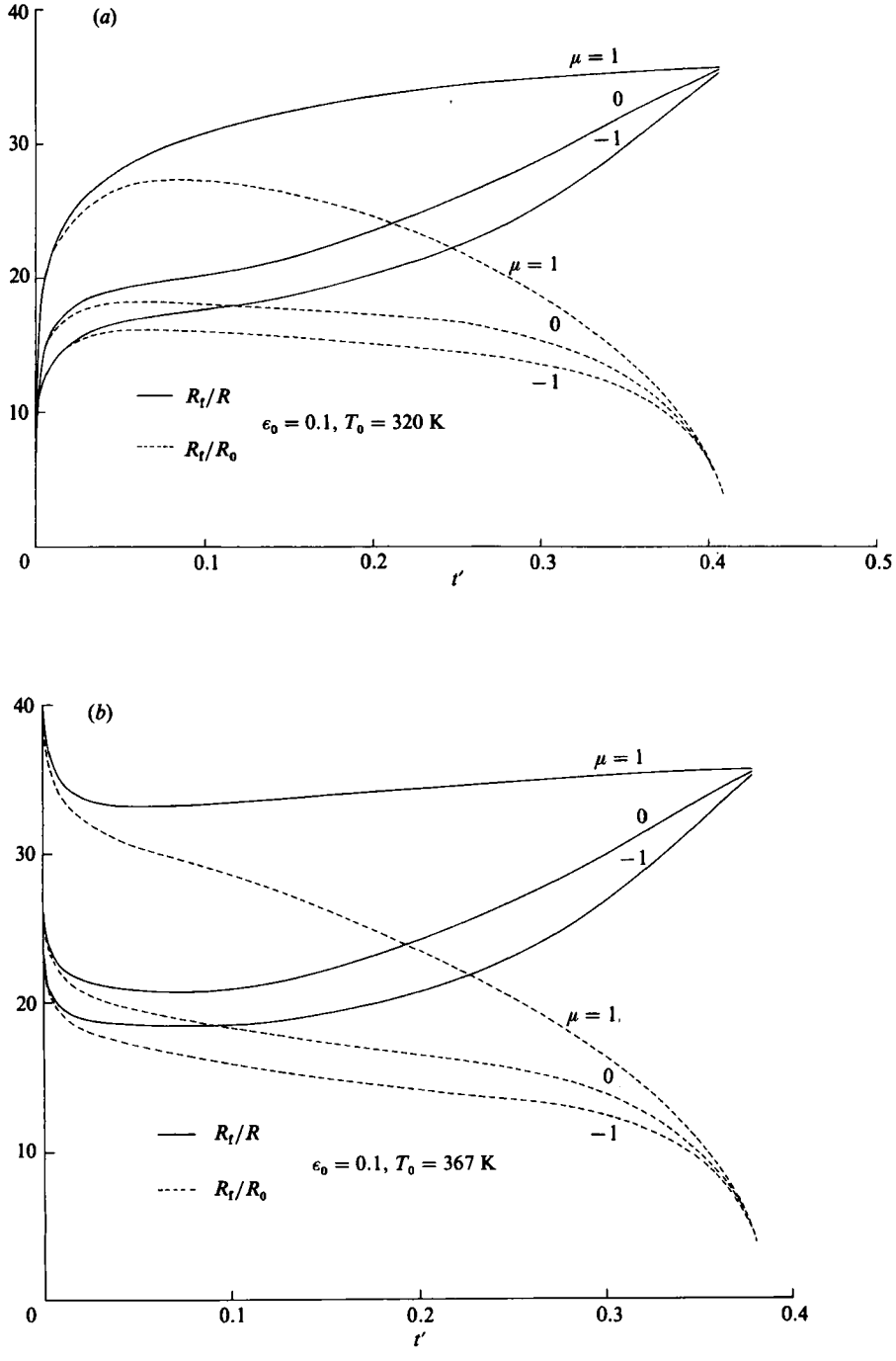

FIGURE 5. Flame distance and flamefront standoff ratio as a function of time at different angular positions: (*a*) $T_0 < T_{wb}$; (*b*) $T_0 > T_{wb}$.

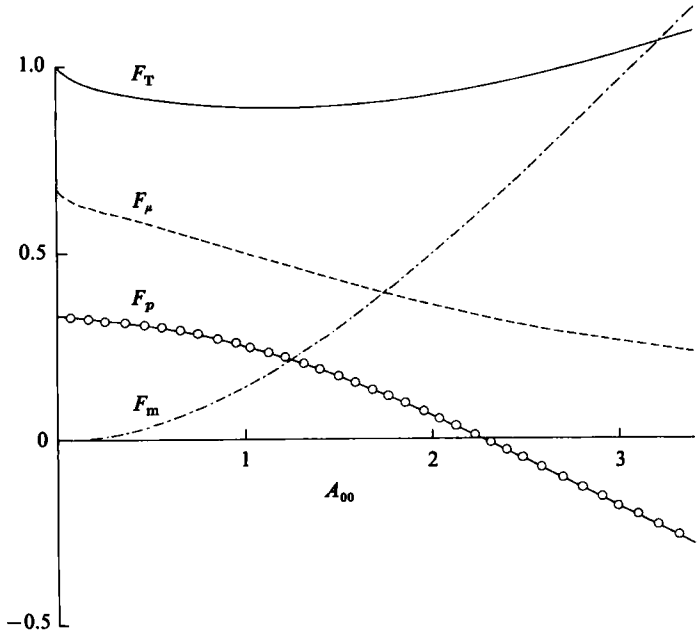

FIGURE 6. The effect of radial field on drag coefficients (density evaluated at reference level).

the front and the rear of the fuel drop. In fact, for a sufficiently large radial velocity, we have a larger pressure at the rear than at the front, thereby causing a negative pressure drag (Sadhal & Ayyaswamy 1983). This is the result of a strong inertial effect due to the maximum radial velocity at the front of the drop. The normal reaction of the momentum flux leaving the surface provides an additional force on the drop. Since the maximum flux is at the front of the drop, the recoil is higher at the front than at the rear. The net effect is an increase in the drag. With increasing A_{00}, this force becomes the dominant effect and results in an increased total drag.

In figure 7 the total drag and its components computed using the variable-density formulation are shown. The total drag calculated from the fixed-density formulation is also shown for comparison. The effect of variable density is to reduce the total drag values further. The feature that, for a certain range of A_{00}, both the fixed and the variable density formulations of this paper predict drag values lower than that of Stokes value is attributable to the proper inclusion of the inertial terms in the development of the theory.

The reduced vorticity at the surface, as discussed earlier, causes the strength $\hat{B}\,Re_\ell$ of the Hill vortex to decrease with increasing A_{00} (figure 8). $\hat{B}$ is given in I for the fixed-density formulation, whereas $\hat{B} = -u_{\theta 1}(1)$ for the variable-density solution. For a given translational velocity, at a sufficiently large radial velocity the internal circulation vanishes. A further increase in A_{00} reverses the circulation. This remarkable result arises from the non-uniformity of the radial field. The interfacial radial velocity increases from the rear towards the front. This introduces a surface shear stress in a sense opposite to that induced by translation. While, with an increasing radial field, the shear stress due to the non-uniformity in the normal velocity persists (see A_{11} and $u_{11}(1)$ in figure 8), the shear stress resulting from translation decreases owing to the convection of vorticity. As a consequence, the internal circulation weakens to a

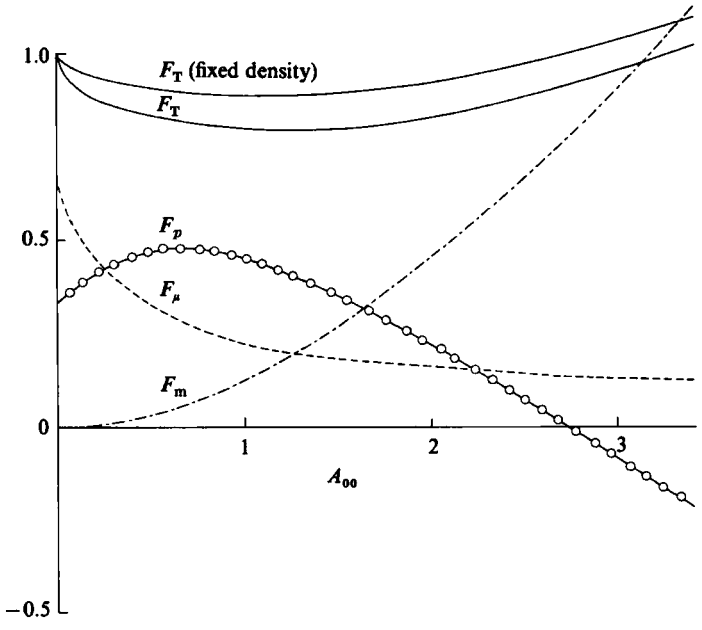

FIGURE 7. The effect of radial field on drag coefficients (variable density).

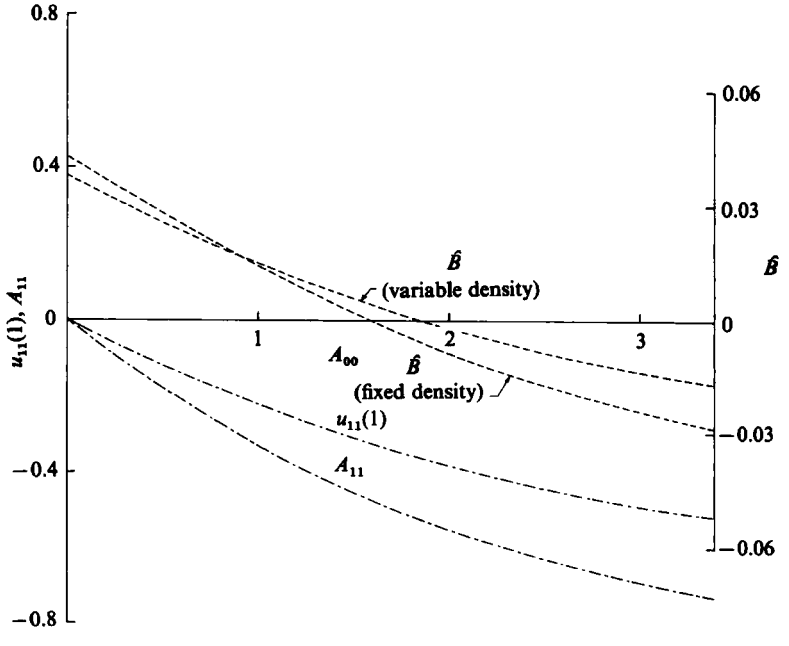

FIGURE 8. The effect of the radial field on liquid circulation, and the extent of non-uniformity $(A_{11}, u_{11}(1))$.

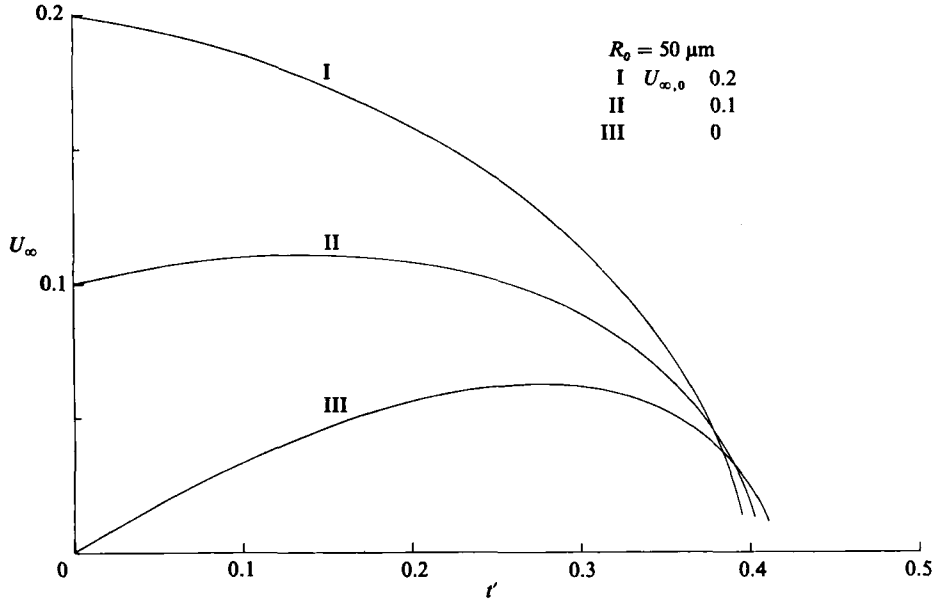

FIGURE 9. Variation in translational velocity with time for a falling burning fuel drop.

point where the shear due to non-uniform evaporation dominates and causes a reversal.

Temporal variations in the instantaneous velocities (equation (31)) for sprayed drops with different injected velocities $U_{\infty,0}$ (I, II), and a free-falling drop (III) are shown in figure 9. Owing to the smallness of the drop considered, the effect of natural convection is negligible. For a free-falling drop the velocity increases to a maximum and decreases thereafter. Initially, the drop weight is greater than the drag force, leading to acceleration. As the drop velocity increases with time, the drag increases and the drop-weight decreases owing to size reduction. When the weight and the drag balance each other, the drop attains its maximum velocity. Subsequently, the drag force overcomes the weight and the drop decelerates. For high enough initial velocities, the drag force overcomes the weight for all times and the drop continuously decelerates. The trends observed in the velocity profiles are in qualitative agreement with the experimental measurements of Wang, Liu & Law (1984).

The fixed- and variable-density models predict that the mass burning is enhanced in the presence of translation. Drop translation enhances the burning rate by convecting the evaporated fuel away from the drop surface and by moving the flame front towards the drop. The driving force is thereby increased, and consequently the burning rate is higher. For an isothermal drop, combining (21*a*, *b*) and (23*b*), we obtain $A_{01} = \frac{1}{2} Sc\, A_{00}$ (after four iterations we find that T_{01} is negligible). Using (27), the mass burning rate is given by $1 + \frac{1}{2} Pe$ ($Pe = U_\infty R/D_g$ is the Péclet number), which is in agreement with Fendell *et al.* (1966). The variable-density solution for the mass burning rate is of a similar form and is given by $\dot{m}/\dot{m}_0 = 1 + \frac{1}{2} Pe_\infty$. It is revealed from the variable-density analysis that for calculating enhancement, property values should be evaluated at free-stream conditions, so long as the assumption of unit Lewis number is invoked. An extensive discussion of experimental results on the

enhancement of the evaporation rate due to translation is available in the studies of Renksizbulut & Yuen (1983*a*, *b*).

This work is based on the doctoral dissertation of George Gogos (1986), carried out in the Department of Mechanical Engineering and Applied Mechanics at the University of Pennsylvania. The authors are very grateful to the Moore School Computing Network for computational facilities and the Dean of Engineering for granting the necessary computer funds. The authors are grateful to two referees who have contributed to the enhancement of the quality of the paper.

REFERENCES

ALDRED, J. W., PATEL, J. C. & WILLIAMS, A. 1971 The mechanism of combustion of droplets and spheres of liquid n-heptane. *Combust. Flame* **17**, 139–148.

BUCKMASTER, J. D. & LUDFORD, G. S. S. 1982 *Theory of Laminar Flames*. Cambridge University Press.

CHUNG, J. N., AYYASWAMY, P. S. & SADHAL, S. S. 1984 Laminar condensation on a moving drop. Part 1. Singular perturbation technique. *J. Fluid Mech.* **139**, 105–130.

FAETH, G. M. 1977 Current status of droplet and liquid combustion. *Prog. Energy Combust. Sci.* **3**, 191–224.

FENDELL, F. E., COATS, D. E. & SMITH, E. B. 1968 Compressible slow viscous flow past a vaporizing droplet. *AIAA J.* **6**, 10, 1953–1960.

FENDELL, F. E., SPRANKLE, M. L. & DODSON, D. S. 1966 Thin-flame theory for a fuel droplet in a slow viscous flow. *J. Fluid Mech.* **26**, 267–280.

GOGOS, G. 1986 Evaporation and combustion of a moving liquid drop. Ph.D. dissertation. University of Pennsylvania, Philadelphia.

KNUTH, E. L. 1959 Multicomponent diffusion and Fick's Law. *Phys. Fluids* **2**, 339–340.

LAW, C. K. 1982 Recent advances in droplet vaporization and combustion. *Prog. Energy Combust. Sci.* **8**, 171–201.

LAW, C. K., CHUNG, S. H. & SRINIVASAN, N. 1980 Gas-phase quasi-steadiness and fuel vapour accumulation effects in droplet burning. *Combust. Flame* **38**, 173–198.

LAW, C. K. & WILLIAMS, F. A. 1972 Kinetics and convection in the combustion of alkane droplets. *Combust. Flame* **19**, 393–405.

RENKSIZBULUT, M. & YUEN, M. C. 1983*a* Experimental study of droplet evaporation in a high-temperature air stream. *Trans. ASME* C: *J. Heat Transfer* **105**, 384–388.

RENKSIZBULUT, M. & YUEN, M. C. 1983*b* Numerical study of droplet evaporation in a high-temperature stream. *Trans. ASME* C: *J. Heat Transfer* **105**, 389–397.

SADHAL, S. S. & AYYASWAMY, P. S. 1983 Flow past a liquid drop with a large non-uniform radial velocity. *J. Fluid Mech.* **133**, 65–81.

SIRIGNANO, W. A. 1983 Fuel droplet vaporization and spray combustion theory. *Prog. Energy Combust. Sci.* **9**, 291–322.

SUNDARARAJAN, T. & AYYASWAMY, P. S. 1984 Hydrodynamics and heat transfer associated with condensation on a moving drop: solutions for intermediate Reynolds numbers. *J. Fluid Mech.* **149**, 33–58.

WANG, C. H., LIU, X. Q. & LAW, C. K. 1984 Combustion and microexplosion of freely falling multicomponent droplets. *Combust. Flame* **56**, 175–197.

WILLIAMS, A. 1973 Combustion of droplets of liquid fuels: a review. *Combust. Flame* **21**, 1–31.

WILLIAMS, F. A. 1985 *Combustion Theory*. Benjamin/Cummings.